Effect of Patch Area and Interaction Length on Clusters and Structures Formed by One-Patch Particles in Thin Systems

ACS OMEGA

http://pubs.acs.org/journal/acsodf

Article

Effect of Patch Area and Interaction Length on Clusters and Structures Formed by One-Patch Particles in Thin Systems

Masahide Sato*

Cite This: https://dx.doi.org/10.1021/acsomega.0c04159

Read Online

ACCESS | Metrics & More | Article Recommendations

ABSTRACT: Assuming that the interaction between particles is given by the Kern−Frenkel potential, Monte Carlo simulations are performed to study the clusters and structures formed by one-patch particles in a thin space between two parallel walls. In isothermal−isochoric systems with a short interaction length, tetrahedral tetramers, octahedral hexamers, and pentagonal dipyramidal heptamers are created with increasing patch area. In isothermal−isobaric systems, the double layers of a triangular lattice, which is the (111) face of the face-centered cubic (fcc) lattice, form when the pressure is high. For a long interaction length, a different type of cluster, trigonal prismatic hexamers, is created. The structures in the double layers also changed as follows: a simple hexagonal lattice or square lattice, which is the (100) face of the fcc structure, is created in isothermal−isobaric systems.

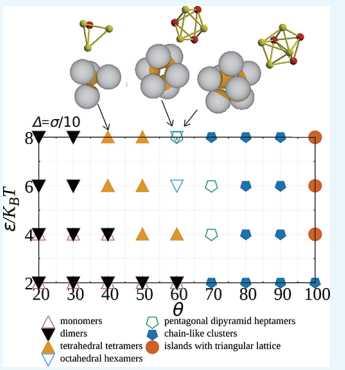

INTRODUCTION

Patchy particles are the particles having several patch areas, whose properties are different from other surface areas. The patchy particles are potential materials because the anisotropy caused by patch areas makes various structures which are not formed by isotropic particles. Many groups[1−33] tried to create various types of self-assemblies with patchy particles. For example, triple helix strings formed by one-patch particles[6] and the kagome lattice formed by triblock Janus spherical particles[7] were observed by Chen and coworkers. Using silica particles with a gold patch, Iwashita and Kimura[17] observed the clusters formed by one-patch particles on a two-dimensional plane. The authors examined how the cluster shape changed and how the ordering of direction of the patch area depended on the size of patch area.

In simulations and theoretical studies,[9,10,14−21,24] the Kern−Frenkel (KF) potential[34] has been often used as the interaction potential between patchy particles. Many kinds of clusters and crystal structures were predicted by controlling the interaction length and the size of the patch area. Previously, assuming that one-patch particles move on a two-dimensional plane rotating three-dimensionally, isothermal−isobaric Monte Carlo (MC) simulations[35] were performed to study the dependence of two-dimensional structures formed by one-patch particles on the interaction length in the KF potential. The author showed that square tetramers, which do not form with a short interaction length, were produced when the interaction length was long.[35]

For one-patch particles in the thin space constructed by two walls, crystal structures and the orientational order of patch direction were studied experimentally.[20,24] In the experiments, the thickness of the space between the two walls changed gradually because the two walls were set to be tilted with a small angle. The structures formed in the thin space depended on the patch area. The orientational order of the direction of patch area changed with the change in crystal structures. MC simulations were also performed by the same papers,[20,24] and the ordering of the direction of patch area was studied for several crystal structures observed in the experiment. The results of the simulations agreed well with those of the experiment. In their simulations,[20,24] however, the orientational order of the direction of patch area was studied only for supposed structures. The possibility of the formation of other structures was not examined, and the reason why the crystal structures observed in their experiment were created is not clear yet.

In previous simulations,[20,24] it was assumed that the interaction length between patchy particles was short. The assumption was reasonable because silica particles with a gold patch were kept in mind as one-patch particles. In a previous study on spherical one-patch particles constructed in a two-dimensional plane,[35] clusters and structures which were not created with a short interaction length formed when the interaction range was long. Also, a study on a free three-dimensional system by another group[21] showed that cluster

Received: August 27, 2020
Accepted: October 21, 2020

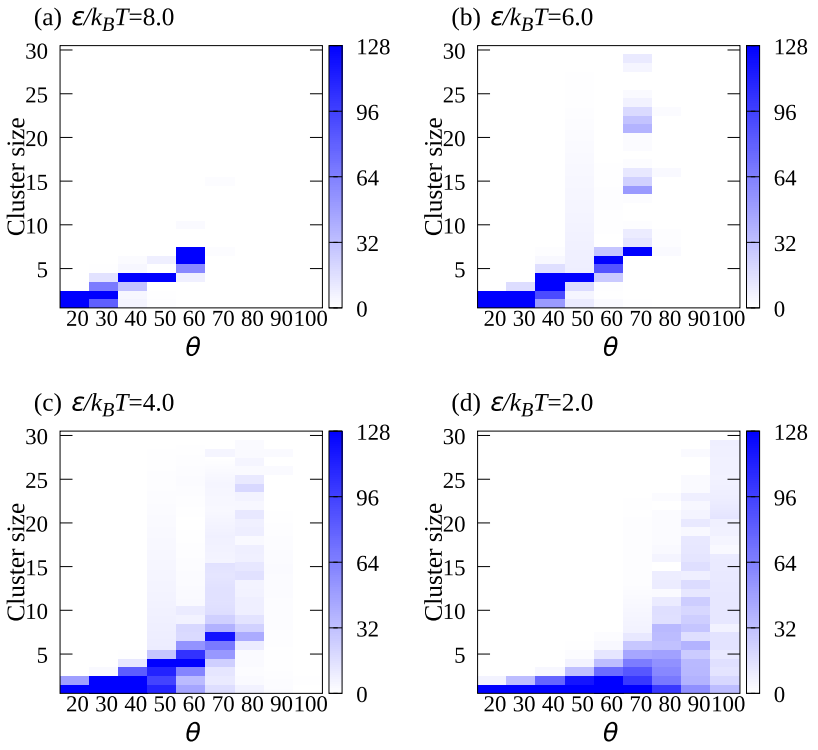

Figure 1. Dependence of the number of clusters on the cluster size and θ for $\Delta = \sigma/10$, where ϵ/k_BT is set to (a) 8.0, (b) 6.0, (c) 4.0, and (d) 2.0. The color bars show $kN(k)$, where $N(k)$ is the number of clusters with the cluster size k.

shapes and crystal structures were strongly affected by the interaction length. Experimentally, long-range interactions may be possible to be synthesized by some fabrication methods. For example, the interaction length may be controlled if DNA strands are used in the patchy area because DNA strands are designed freely.[36−53] Thus, it is also interesting to study how the interaction length affects clusters and structures formed by patchy particles in thin systems.

In this paper, considering the spherical one-patch particles constructed in the thin space between two parallel walls, how the cluster types and structures formed by one-patch particles depend on the patch area and the interaction length is studied. First, the model used is introduced. Second, the results of the simulations are shown. Isothermal−isochoric MC simulations are performed in dilute systems to show how the cluster shape depends on the interaction length, the interaction strength, and the patch area. Then, isothermal−isobaric MC simulations are performed and how the structures formed by one-patch particles change with pressure is shown. Finally, the results are summarized in Conclusions.

■ RESULTS AND DISCUSSION

In the simulations, the z-axis is set perpendicular to the two parallel walls and the xy-plane is parallel to them. The periodic boundary conditions are used in both x- and y-directions. In constructed systems, walls affect structures formed by the particles with an isotropic interaction. The structures which are not expected by the free three-dimensional system are reported[54−59] when the distance between the two walls is smaller than twice the value of the particle diameter. To avoid the strong effect of walls, the distance between the two parallel walls l_z is set to 2.1σ, which is a little larger than twice the value of the particle diameter. The number of particles used in the simulations N is 512. The diameter of the particles σ is set to unity.

Clusters Forming in Isothermal−Isochoric Systems. First, by performing isothermal−isochoric MC simulations, the dependence of the cluster size on the interaction energy, the interaction length, and the patch area is studied for a short interaction length. The particle density $\pi\sigma^3N/(6l_xl_yl_z)$ and the interaction length Δ are set to 0.2 and $\sigma/10$, respectively. The relationship between θ and cluster types is examined by changing θ every 10° from 20 to 100° for ϵ/k_BT = 8.0, 6.0, 4.0, and 2.0. Initially, particles are put at random. In one MC trial, the translation and rotation are tried for one particle. To avoid making the success rate of MC trials too low, the maximum values of translation and rotation of particles are tuned every $100N$ MC trials.[60]

Clusters with a Short Interaction Length. Figure 1 shows how the number of clusters depends on θ and the cluster size, that is, the number of particles in a cluster. The color strength is proportional to $kN(k)$, where $N(k)$ is the number of clusters with the cluster size k. $N(k)$ is averaged over 10 times every 10^6N MC trials after $3N \times 10^7$ MC trials. For ϵ/k_BT = 8.0 Figure 1a), the distribution of the cluster size is narrow as the effect of thermal fluctuations is small, and the appropriate cluster size is determined by the patch area. For $\theta < 60°$ or $\chi < 2.5 \times 10^{-1}$, the cluster size increases with increasing θ. When $\theta \geq 70°$ or $\chi \geq 3.3 \times 10^{-1}$, the clusters smaller than 30 particles are not seen because many particles assemble and long string-like clusters form.

For ϵ/k_BT = 6.0 (Figure 1b), the distribution of cluster size is similar to that for ϵ/k_BT = 8.0 when $\theta \leq 60°$, but the distribution is broader than that with ϵ/k_BT = 8.0 and various sizes of clusters from when θ = 70°. The formation of these clusters is caused by thermal fluctuations. As they make the rotation and translation of particles frequent, the connections in clusters are cut easily

https://dx.doi.org/10.1021/acsomega.0c04159
ACS Omega XXXX, XXX, XXX−XXX

and the long string-like clusters are broken into small clusters. For $\epsilon/k_BT = 4.0$ (Figure 1c) and $\epsilon/k_BT = 2.0$ (Figure 1d), the distribution starts to be broad with a small θ owing to the further increase in the effect of thermal fluctuations.

Figure 2 shows several typical snapshots for $\epsilon/k_BT = 8.0$, where the system is seen from the positive z-direction. Figure 3

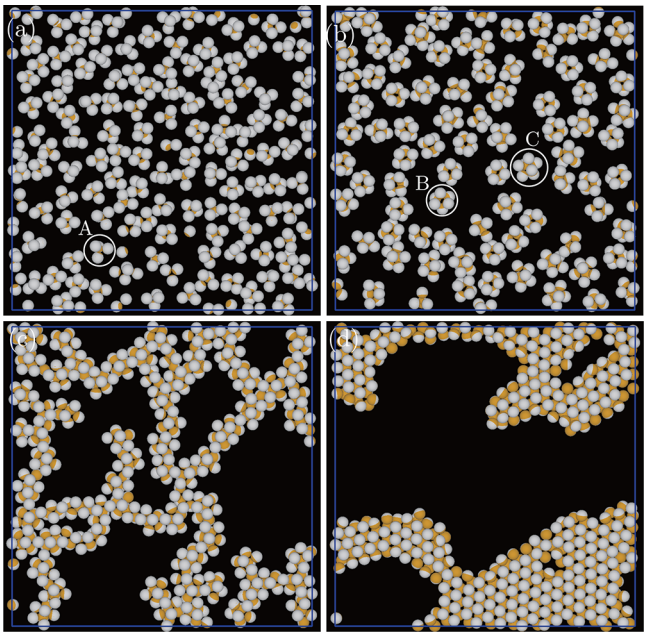

Figure 2. Typical snapshots for a short interaction length, where $\epsilon/k_BT = 8.0$ and θ is set to (a) 40, (b) 60, (c) 70, and (d) 100°. χ is given by (a) 1.7×10^{-1}, (b) 2.5×10^{-1}, (c) 3.3×10^{-1}, and (d) 5.9×10^{-1}. The interaction length is set to $\Delta = \sigma/10$.

shows the zoomed snapshots of several clusters in Figure 2. When $\theta = 40°$ or $\chi = 1.2 \times 10^{-1}$ (Figure 2a),most numerous clusters are tetrahedral tetramers such as A (Figure 3A). As l_z is set to 2.1σ in the simulations, l_z is large enough for the

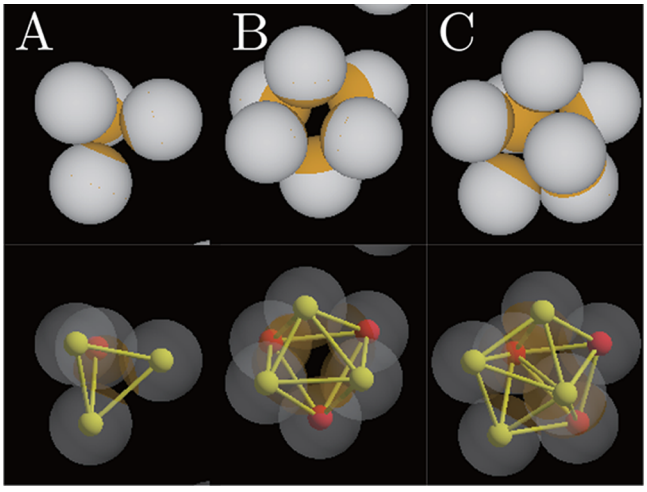

Figure 3. Zoomed snapshots for clusters (A−C) in Figure 2. The upper figures show the zoomed snapshots for the clusters. The lower figures show the connections in the clusters, where the connections are drawn with yellow lines. Red and yellow particles are put at the centers of patchy particles whose z-coordinates are larger and lower than $L_z/2$, respectively.

tetrahedral tetramers to rotate freely in the thin space. Thus, the tetrahedral tetramers orient in many directions. For the KF potential,[34] the interaction energy is simply proportional to the number of interacting particles. As each particle in the observed tetrahedral tetramers interacts with other three particles, the interaction energy per particle for the tetrahedral tetramers, U_4, satisfies $U_4/k_BT = -3\epsilon/(2k_BT) = 12.0$.

When $\theta = 60°$ or $\chi = 2.5 \times 10^{-1}$ (Figure 2b), two types of clusters, octahedral hexamers such as B (Figure 3B) and pentagonal dipyramidal heptamers such as C (Figure 3C), coexist in the system. For the octahedral hexamers, each particle in a cluster connects with other four particles, while for the pentagonal dipyramidal heptamers, each particle in the pentagonal plane connects with four neighboring particles and the two vertexes connect with all the particles in the pentagonal plane. The interaction energies per particle for the octahedral hexamers, U_6, and the pentagonal dipyramidal heptamers, U_7, satisfy $U_6/k_BT = -2\epsilon/(k_BT) = 16.0$ and $U_7/k_BT = -3\epsilon/(k_BT) = 24.0$. As the number of connections per particle in the pentagonal dipyramidal heptamers is slightly larger than that in the octahedral hexamers, the pentagonal dipyramidal heptamer is considered to be more energetically favorable than the octahedral hexamer. However, the latter was more numerous than the former: the average numbers of octahedral hexamers and pentagonal dipyramidal heptamers were 45 and 24, respectively.

The unexpected relationship between the two cluster numbers is caused by small l_z. When one of the triangular planes in octahedral hexamers is parallel to the xy-plane as observed in my simulations, the octahedral hexamers have enough space in the z-direction. Thus, they can move without bumping against the walls by thermal fluctuations. On the other hand, the pentagonal planes in the pentagonal dipyramidal heptamers are a bit tilted from the xy-plane, as seen in Figure 2b, which means that l_z is too narrow compared with the distance between two vertexes of the pentagonal dipyramidal heptamers and that the heptamers probably bump against the walls with a small motion. Thus, the dipyramidal heptamers cannot move freely in the systems and may be easily broken by thermal fluctuations.

When $\theta = 70°$ or $\chi = 3.3 \times 10^{-1}$ (Figure 2c), one large cluster is created. The shape of this cluster is like a mesh formed by meandering strings. The z-coordinates of particles are separated into two levels. The patch direction of almost all the lower side particles is the positive z-direction and that of almost all the upper side particles is the negative z-direction. Taking into account the patch area, it can be observed that the particles cannot connect with the neighbors in the same z-level as the patch direction is parallel to the z-axis.

The mesh-like pattern formed by string-like clusters is also created for $\theta = 80$ and 90°. The cluster shape is different from the string-like one for $\theta = 100°$ or $\chi = 5.9 \times 10^{-1}$ (Figure 2d): the cluster shape becomes compact and the number of voids decreases compared with that in Figure 2c. As the system sizes in our simulations are not so large, all the particles gather and one large island with some voids is created. As the patch area is sufficiently large, the particles can connect with the neighbors at the same z-level. The particles in each z-level make a triangular lattice to increase the number of connected particles as much as possible. In the triangular lattice, particles connect with nine particles, six particles in the same z-level and three particles in a different z-level. The interaction energy per particle U_Δ satisfies $U_\Delta/k_BT = -9\epsilon/(2k_BT) = 36.0$.

https://dx.doi.org/10.1021/acsomega.0c04159
ACS Omega XXXX, XXX, XXX−XXX

The effect of thermal fluctuations on the cluster shape for string-like clusters is shown. Figure 4 shows snapshots (Figure 4a,c) and the connections between particles (Figure 4b,d) with ϵ/k_BT = 6.0 and 4.0 for θ = 70°. A long string-like cluster forms when ϵ/k_BT = 8.0 (Figure 2c), but the cluster shape becomes short when ϵ/k_BT = 6.0 (Figure 4a,b). The short string-like clusters seem to be formed by the connection of a few pentagonal dipyramidal heptamers. For ϵ/k_BT = 4.0 (Figure 4c,d), the size of string-like clusters is smaller than that with ϵ/k_BT = 6.0 and the form of the unit of sting-like clusters becomes obscure as the effect of thermal fluctuations increases.

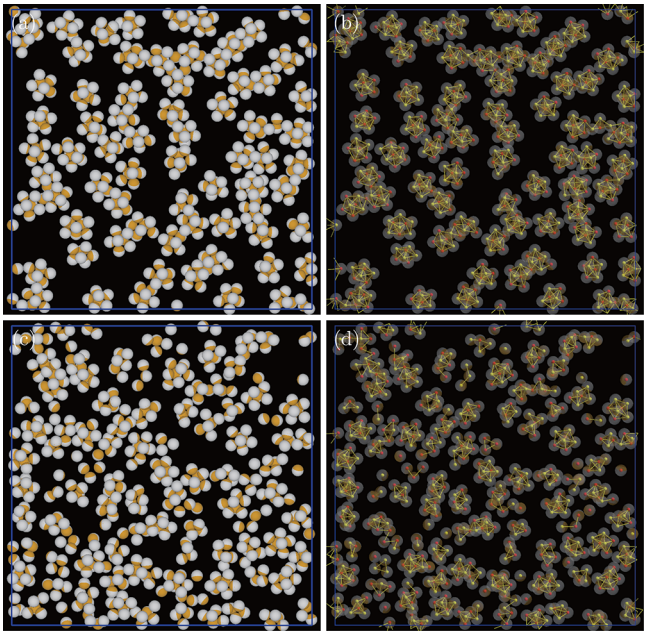

Figure 4. Typical snapshots and connections between particles in these snapshots with θ = 70° for $\Delta = \sigma/10$. ϵ/k_BT is 6.0 (a,b) and 4.0 (c,d). The connections are drawn with yellow lines. In (a,b), the orange area is the patch area. In (c,d), red particles and yellow particles are put at the centers of patchy particles in the lower and upper regions, respectively.

Clusters with a Long Interaction Length. In a previous study,[35] the author studied how the two-dimensional structures formed by one-patch particles depend on the interaction length. When the interaction length is $\Delta = \sigma/2$ and the pressure is low, two types of square tetramers form, which are not created with a short interaction length. Here, assuming that $\Delta = \sigma/2$ simulations are performed to study how the interaction length affects the cluster shape in thin systems.

First, how the distribution of cluster size depends on the interaction length is examined. Figure 5 shows the distribution of cluster size for the long interaction length. For ϵ/k_BT = 2.0 (Figure 5c) and ϵ/k_BT = 4.0 (Figure 5d), the distributions seem to be similar to those with the short interaction length (Figure 1c,d). On the other hand, for ϵ/k_BT = 8.0 (Figure 5a) and 6.0 (Figure 5b), the distributions are broader and clusters forming with the long interaction length are larger, compared to the system with a sticky type of short interaction length.

To clarify the effect of the difference in the interaction length in more detail, snapshots for ϵ/k_BT = 8.0 in Figure 6 and also zoomed snapshots of several clusters observed in Figure 7are shown. When $\theta \leq 30°$ or $\chi = 6.7 \times 10^{-2}$, polyhedral clusters hardly form, and dimers and trimers from instead. As the polyhedral clusters also do not form in systems with a short interaction length, the effect of the difference in the interaction length on the cluster shape is small in this θ region. When $\theta = 40°$ or $\chi = 1.2 \times 10^{-1}$ (Figure 6a), trigonal prismatic hexamers such

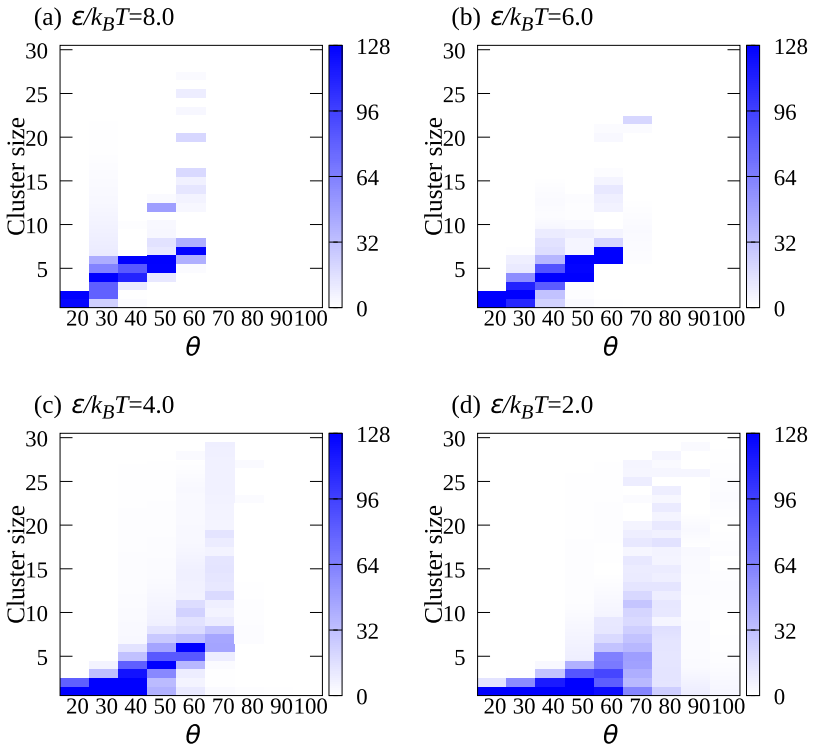

Figure 5. Dependence of the number of clusters on the cluster size and θ for $\Delta = \sigma/2$, where ϵ/k_BT is set to (a) 8.0, (b) 6.0, (c) 4.0, and (d) 2.0. The color bars show $kN(k)$, where $N(k)$ is the number of clusters with the cluster size k.

https://dx.doi.org/10.1021/acsomega.0c04159
ACS Omega XXXX, XXX, XXX−XXX

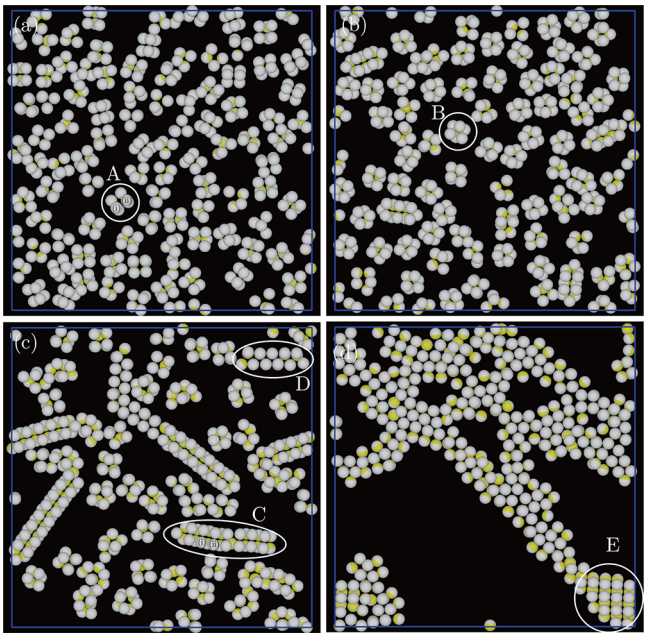

Figure 6. Typical snapshots for $\Delta = \sigma/2$, where $\epsilon/k_BT = 8.0$ and θ is set to (a) 40, (b) 50, (c) 60, and (d) 80°. Yellow area represents the patch area.

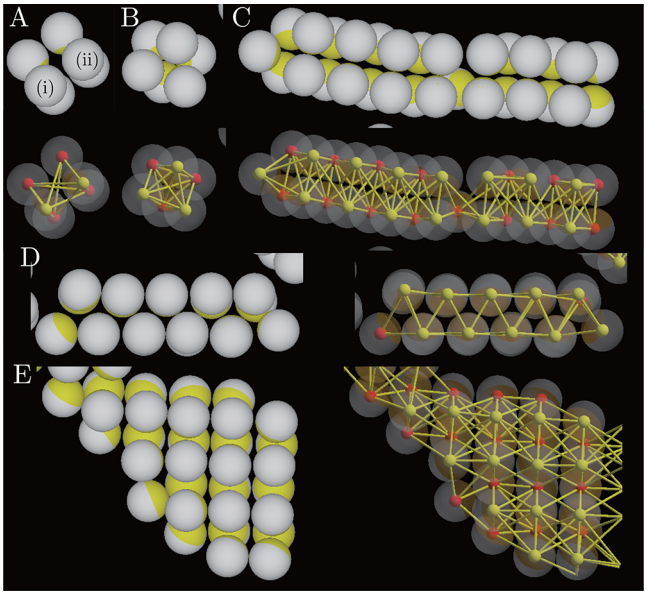

Figure 7. Zoomed snapshots for clusters (A−E) shown in Figure 6, where the connections in the clusters are also shown by yellow lines. Red and yellow particles are put at the centers of patchy particles whose z-coordinates are larger and lower than $L_z/2$, respectively.

as A, which are not observed in systems with a short interaction length (Figure 2a), are created. In cluster A (Figure 7A), particle (i) connects with all the other particles in the same cluster expect for particle (ii) as the interaction length Δ is long. Thus, the interaction energy per particle, U_{6p}, satisfies $U_{6p}/k_BT = -5\epsilon/(2k_BT) = 20.0$, which is larger than U_6.

The number of connections per particle is four in the cluster. Hexamers also form when $\theta = 50°$ (Figure 6b), but their shape is a tetrahedron such as B (Figure 7B). Owing to the increase in the patchy area, each particle in the cluster connects with all the other particles. As the number of connections per particle is five, the tetrahedral clusters are energetically preferred to the trigonal prismatic clusters.

When $\theta = 60°$ or $\chi = 2.5 \times 10^{-1}$ (Figure 6c), clusters like the chains of trigonal prismatic form. As l_z is not too small, both types of clusters such as C (Figure 7C) and D (Figure 7D) form. In cluster C, particle (i) does not connect with particle (ii) because the patch area is not so large. The number of connections per particle is five in both C and D. The difference in these two types of clusters is the orientation; the type of C is the same as that of D when cluster C is rotated by 90°. These two types of clusters are energetically equivalent to each other.

When $\theta = 80°$ or $\chi = 4.1 \times 10^{-1}$ (Figure 6d), one large cluster, which seems to be an island with a few large voids, is created. This cluster consists of a region with a simple hexagonal lattice and region E (Figure 7E). Taking into account the patch area and the interaction length, the number of connections per particle is estimated to six in region E and seven in the simple hexagonal lattice. As the region with the simple hexagonal lattice is more energetically favorable than region E, it is reasonable that the area of the former region is larger than that of the latter region. Because the system size is not so large in our simulations, only one island is created in the systems. If simulations are performed in larger systems, some island-like clusters consisting of the mixture of the hexagonal lattice and the structure such as region E should be created.

How the types of mainly formed clusters change with ϵ/k_BT and θ is summarized in Figure 8, where the cluster types remarked in the snapshots are indicated for each set of parameters. When $\Delta = \sigma/10$ (Figure 8a), the θ region with dimers increases with decreasing ϵ/k_BT. When $\epsilon/k_BT \leq 4.0$, the monomers are included in the region with dimers. As the interaction energy is not sufficiently large, the creation and separation of dimers are probably repeated in these energies. When $\epsilon/k_BT > 2.0$, polygonal clusters with clear shapes are created when $40° < \theta < 70°$. When $\theta = 60^{\theta}$ and $\epsilon/k_BT = 8.0$, octahedral hexamers and pentagonal dipyramidal heptamers are created as we have already shown in Figure 2b; when $\epsilon/k_BT = 2.0$, those polygonal clusters do not form and the region with monomers and dimers expands. Island-like clusters are not created and the connection between particles in chain-like clusters is looser than that with $\epsilon/k_BT > 2.0$. When $\Delta = \sigma/2$ (Figure 8b), trigonal prismatic clusters, which are not observed for $\Delta = \sigma/10$, are created with $\epsilon/k_BT = 8.0$ because of the long interaction length. As the long interaction length makes the connection between particles easier, polygonal clusters become looser than those with the short interaction length. Thus, the shapes of hexamers and tetramers are irregular with $\epsilon/k_BT \leq 6.0$. Another effect of the long interaction length is to increase the region with island-like clusters. The structure in the island-like clusters is the mixture of a simple hexagonal structure and a square lattice, while the island-like clusters consist of a triangular lattice with a short interaction length.

Structures Forming in Isothermal−Isobaric Systems. In previous sections, isothermal−isochoric MC simulations are performed and the dependence of cluster shape on θ and ϵ/k_BT is studied. Hereafter, performing MC simulations controlling pressure, how structures formed by one-patch particles in a thin space depend on the interaction energy and pressure is studied. In the simulations, the scaled pressure $P\sigma^3/k_BT$ is changed every 5 from 5 to 50. Initially, the particle density is set to 0.2 and the particle positions are at random. During the simulations, the lengths of systems in x- and y-directions are changed isotropically in each MC trial, while l_z is kept as 2.1σ.

https://dx.doi.org/10.1021/acsomega.0c04159
ACS Omega XXXX, XXX, XXX−XXX

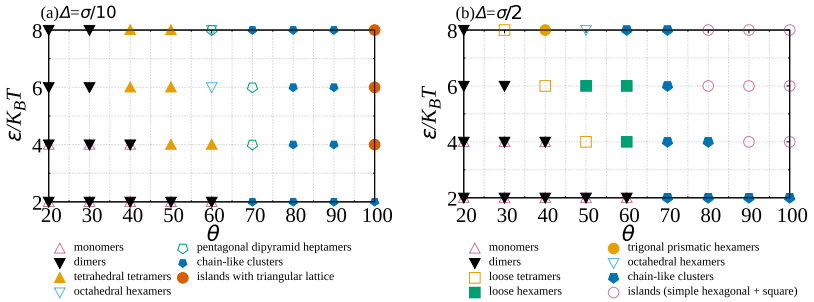

Figure 8. Dependence of the cluster type on ϵ/k_BT and θ for (a) $\Delta = \sigma/10$ and (b) $\Delta = \sigma/2$.

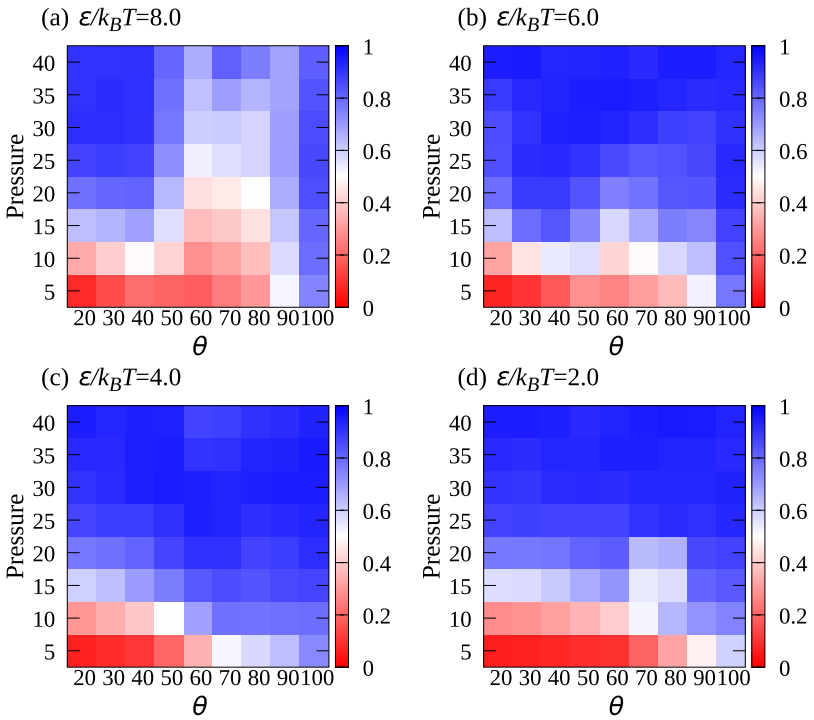

Figure 9. Dependence of ϕ_6 on $P\sigma^3/k_BT$ and θ for $\Delta = \sigma/10$, where ϵ/k_BT is set to (a) 8.0, (b) 6.0, (c) 4.0, and (d) 2.0. The color bars show the value of ϕ_6.

Structures Forming in Isothermal−Isobaric Systems with a Short Interaction Length. If the pressure is sufficiently high and the interaction length Δ is short, the double layers of a triangular lattice, which is the same as the (111) face of the face-centered cubic (fcc) lattice, should be formed to make the particle density high. In each plane, the six-fold rotational symmetry is expected to be high if the triangular lattice is created. Thus, to estimate the six-fold rotational symmetry, ϕ_6 is introduced, which is given by

$$\phi_6 = \frac{1}{N}\sum_i \left| \frac{1}{n_N(i)} \sum_j{}' \exp(i6\theta_{ij}) \right| \quad (1)$$

where $n_N(i)$ is the number of neighboring particles in the same z-level for the ith particle, θ_{ij} represents the angle between $\boldsymbol{r}_{ij}$ and the x-axis, and $\sum_j'$ is the summation of the neighboring particles in the same z-level. In the simulations, the ith and jth particles are considered to be in the same z-level when the difference in their z-coordinates is smaller than 0.2σ, and the ith and jth particles are regarded as neighbors when r_{ij} is smaller than 1.1σ. The interaction length is $\sigma/10$ as a short interaction length.

Figure 9 shows the dependence of ϕ_6 on $P\sigma^3/k_BT$ and θ. When ϵ/k_BT is small, which means that the effect of thermal fluctuations is large (Figure 9d), ϕ_6 is large in the high-pressure region. With the increase of the interaction energy, the region with small ϕ_6 decreases because particles aggregate easily owing to the attractive interaction, especially in the large θ region (Figure 9c). However, with a further increase in ϵ/k_BT, ϕ_6 starts to decrease again (Figure 9a,b) in the low-pressure region. When $\epsilon/k_BT = 8.0$ (Figure 9a), the increase in the low ϕ_6 region is remarked for $50^\circ \le \theta \le 90^\circ$ or $1.8 \times 10^{-1} \le \chi \le 0.5$. The decrease in ϕ_6 in this θ region is related to the anisotropy in the attractive interaction. The clusters such as octahedral hexamers and pentagonal dipyramidal heptamers form in this θ region. These clusters do not have the six-fold symmetry, and they are stable because the number of connections per particle is large. Thus, it is hard to break them, and a large pressure is necessary to form the triangular lattice with a large ϕ_6.

For $\epsilon/k_BT = 8.0$, the change in ϕ_6 is more drastic than that with other interaction energies. To clarify the relationship between ϕ_6 and the structures formed in the systems with this energy, several typical snapshots for $\epsilon/k_B = 8.0$ are shown in Figure 10 and the interactions between particles in Figure 11.

https://dx.doi.org/10.1021/acsomega.0c04159
ACS Omega XXXX, XXX, XXX−XXX

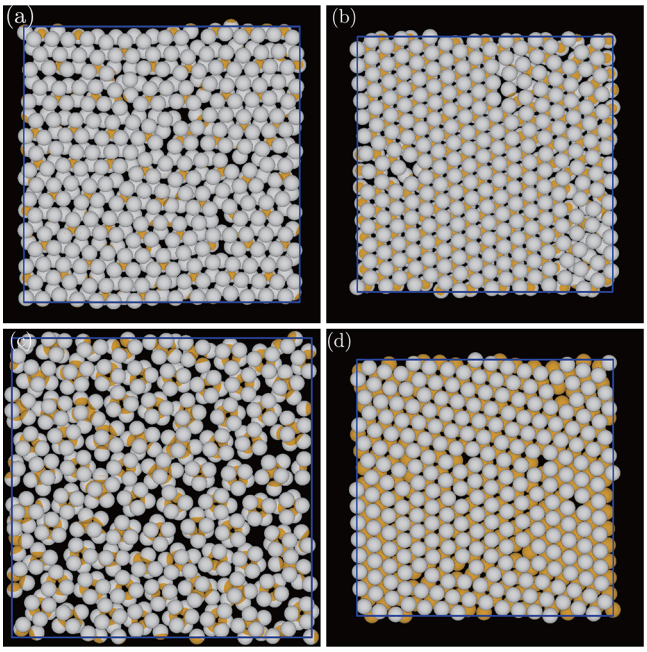

Figure 10. Typical snapshots for $\Delta = \sigma/10$, where $\epsilon/k_BT = 8.0$ and θ and $P\sigma^3/k_BT$ are, respectively, set to (a) 40° and 10, (b)40° and 30, (c) 60° and 5, and (d) 100° and 35. χ is given by (a,b) 1.2×10^{-1}, (c) 2.5×10^{-1}, and (d) 5.9×10^{-1}. Orange area represents the patch area.

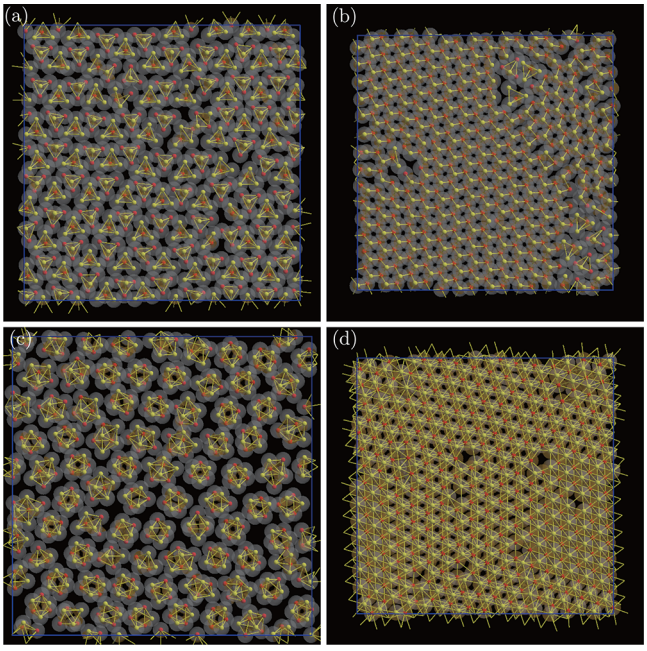

Figure 11. Interactions between particles in Figure 10, where θ and $P\sigma^3/k_BT$ are, respectively, set to (a) 40° and 10, (b) 40° and 30, (c) 60° and 5, and (d) 100° and 35. χ is given by (a,b) 1.2×10^{-1}, (c) 2.5×10^{-1}, and (d) 5.9×10^{-1}. Yellow lines represent connections between particles. Red particles and yellow particles are put at the centers of patchy particles in the lower and upper regions, respectively.

For $\theta = 40°$ or $\chi = 1.2 \times 10^{-1}$, and $P\sigma^3/k_BT = 10$, a snapshot is shown in Figure 10a and the connections between particles in Figure 11a. From these figures, one can find that tetrahedral tetramers form in the system with these parameters. ϕ_6 should be large if the tetrahedral tetramers are arranged regularly, but ϕ_6 is low in the simulations because the pressure is not too large to enable the tetramers placed in a regular manner.

When θ is kept the same and $P\sigma^3/k_BT$ is increased (Figure 10b), the double layers of a triangular lattice with a large ϕ_6, which is the same as the (111) face of the fcc lattice, are created. The connections between particles in this system shown in Figure 11b are quite different from those with low pressures shown in Figure 11a: the connections in tetrahedral tetramers are broken and almost all the particles connect with their three nearest neighbors in the different z-level, while in both structures, the number of interacting particles per particle is three and the interaction energy is estimated as $3\epsilon/(2k_BT) = 12.0$. When $\theta = 60°$ or $\chi = 2.5 \times 10^{-1}$, and $P\sigma^3/k_BT = 5$ (Figures 10c and 11c), many octahedral hexamers and a few pentagonal dipyramidal heptamers form. These clusters are stable as the number of connections per particle is large. As the rotational symmetry of pentagonal dipyramidal heptamers is not six-fold, the regular triangular lattice does not form easily, so that ϕ_6 is low even with high pressures.

For $\theta = 100°$ or $\chi = 5.9 \times 10^{-1}$ (Figures 10d and 11d), the patch area is so large that the particles can attract not only particles in the different z-level but also those in the same z-level if the patch direction is almost parallel to the z-axis. When the double layers of the triangular lattice form, the number of connections per particle is nine: the connections with the particles in the same z-level are six and those with the particles in the different z-level are three. Thus, the interaction energy per particle is estimated as $9\epsilon/(2k_BT) = 36.0$. As the number of connections is large, the double layers of the triangular lattice are created even with low pressures.

In previous studies,[20,24] structures formed by one-patch particles in thin systems were studied. The system width was thinner than our simulations, but the double layers of the triangular lattice were observed. In the systems, the structure given by Figure 10b and the regular structure formed by octahedral hexamers are created. In those studies, the structures formed by patchy particles with $\theta > 90°$ were not studied. However, if experiments are performed with patchy particles with $\theta > 90°$, the structure such as in Figure 10d may be observed.

Structures Forming in Isothermal−Isobaric Systems with a Long Interaction Length. We also examine what kinds of structures form in the thin systems for $\Delta = \sigma/2$ and show how the interaction length affects the structures created in the systems. Figure 12 shows how ϕ_6 depends on $P\sigma^3/k_BT$ and θ. For $\epsilon/k_BT = 2.0$ (Figure 12d), ϕ_6 is small with low pressures and the dependence of ϕ_6 on θ seems to be small. Except that ϕ_6 is small in the small pressure region even with a large θ, and the difference between Figures 12d and 9d is small.

For $\epsilon/k_BT = 4.0$ (Figure 12c), ϕ_6 is small when θ is small and the pressure is low or when $\theta = 100°$. Small ϕ_6 with a low pressure and a small θ is also observed for the short interaction length (Figure 9c), but a small ϕ_6 with $\theta = 100°$ is observed only for the long interaction length. ϕ_6 is also small in these two regions for larger energies, and the areas with a small ϕ_6 spread with increasing ϵ/k_BT (Figure 12a,b).

Several snapshots are shown to clarify why ϕ_6 change, as shown in Figure 12, and how ϕ_6 is related to the structures created in the thin systems. Figures 13 and 14 show snapshots with $\epsilon/k_BT = 8.0$ for a long interaction length and the connections between particles in these snapshots, respectively. For $\theta = 20°$ or $\chi = 3.0 \times 10^{-2}$ (Figure 13a), double layers of triangular lattices are created when the pressure is high. These

https://dx.doi.org/10.1021/acsomega.0c04159
ACS Omega XXXX, XXX, XXX−XXX

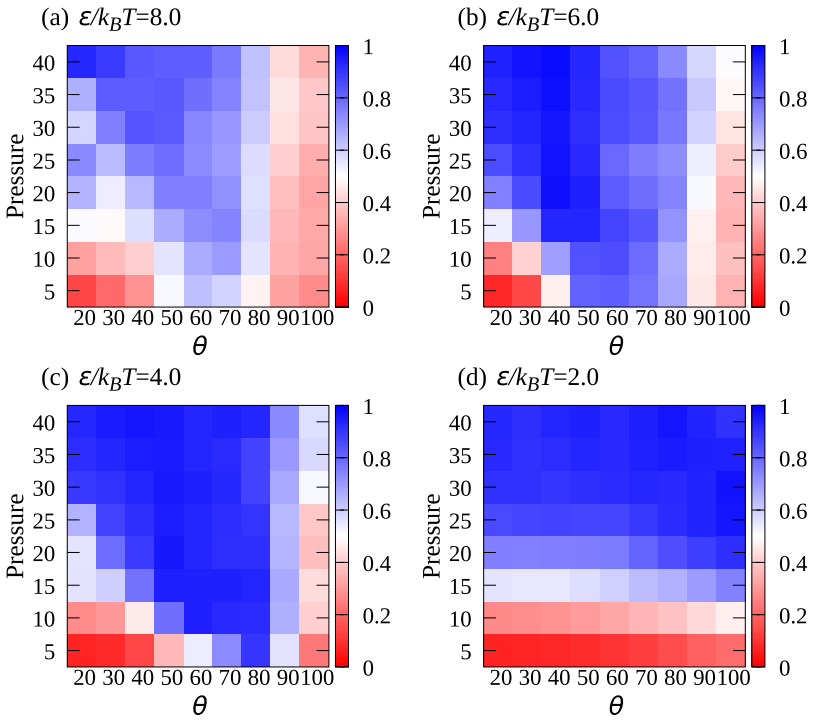

Figure 12. Dependence of ϕ_6 on $P\sigma^3/k_BT$ and θ for $\Delta = \sigma/2$, where ϵ/k_BT is set to (a) 8.0, (b) 6.0, (c) 4.0, and (d) 2.0. The color bars show the value of ϕ_6.

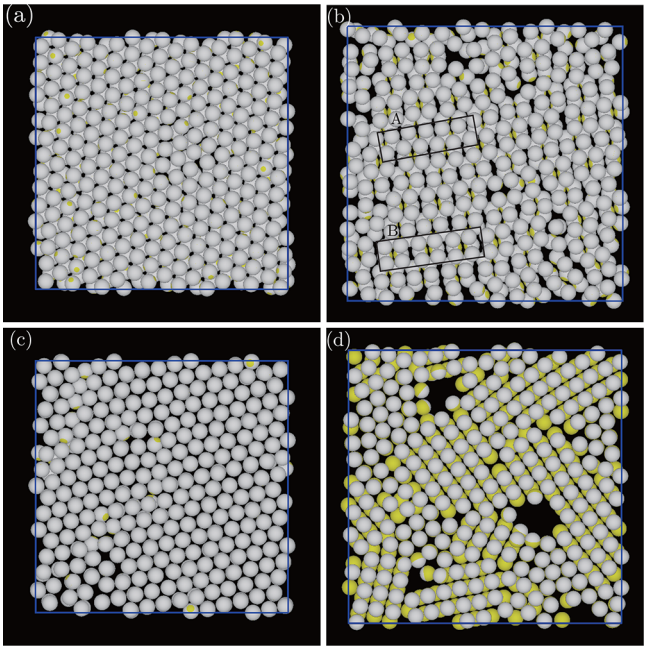

Figure 13. Typical snapshots for $\Delta = \sigma/2$, where $\epsilon/k_BT = 8.0$, and θ and $P\sigma^3/k_BT$ are, respectively, given by (a) 20° and 40, (b) 30° and 10, (c) 30° and 40, and (d) 100° and 10. χ is given by (a) 3.0×10^{-2}, (b,c) 6.7×10^{-2}, and (d) 5.9×10^{-1}. Yellow area represents the patch area.

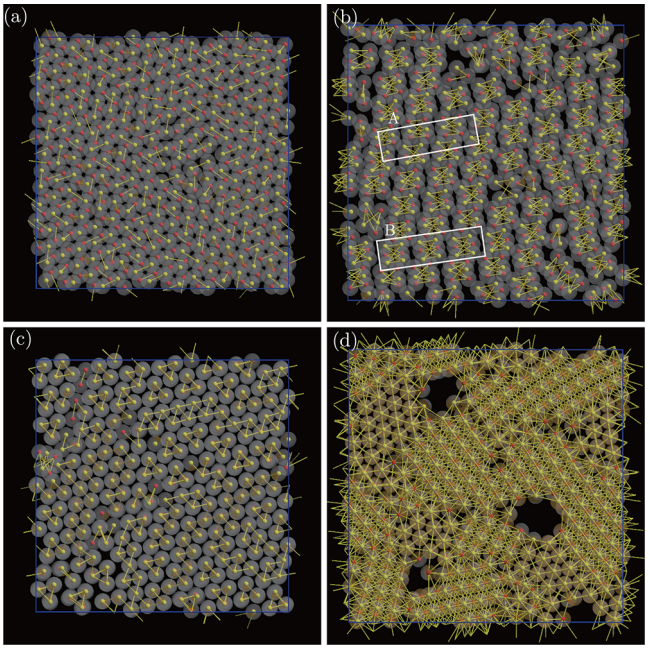

Figure 14. Interactions between particles in Figure 13, where θ and $P\sigma^3/k_BT$ are, respectively, given by (a) 20° and 40, (b) 30° and 10, (c) 30° and 40, and (d) 100° and 10. χ is given by (a) 3.0×10^{-2}, (b,c) 6.7×10^{-2}, and (d) 5.9×10^{-1}. Red particles and yellow particles are put at the centers of patchy particles in the lower and upper regions, respectively.

double layers are the (111) face of the fcc lattice, which is the same as that formed for $\Delta = \sigma/10$. As particles in the double layers form dimers, the interaction energy per particle is given by $\epsilon/(2k_BT) = 4.0$. The directions of the connections between particles are at random as shown in Figure 14a.

For $\theta = 30°$ or $\chi = 6.7 \times 10^{-2}$, with a low pressure (Figure 13b), the double layers are created, but their structures are more irregular than those in Figure 13a: the mixture of short rows of triangles such as A (Figure 13b) and those of squares such as B (Figure 13b) forms in a plane. The cause of the formation of these structures is evident when one sees the connection of particles in the thin system. As shown in Figure 14b, the mixture of those rows is created by trigonal prismatic hexamers, whose shape is the same as that of cluster A in Figure 6a. The normal

https://dx.doi.org/10.1021/acsomega.0c04159
ACS Omega XXXX, XXX, XXX−XXX

directions of the bases of almost all the trigonal prismatic hexamers are in the *xy*-plane. As the rows of prismatic hexamers one of whose side faces appears in the lower layer and in the upper layer alternatively, the rows of triangles such as A (Figures 13b and 14b) and those of squares such as B (Figures 13b and 14b) are created.

If the pressure is slightly larger, arrays of the trigonal prismatic hexamers probably become more regular, and the long rows of triangles and those of squares should appear alternatively. However, when the pressure becomes further higher in Figures 13c and 14c, those arrays of triangular prismatic hexamers are broken, and the double layers of a simple hexagonal lattice, whose structure is the same as D in Figure 6c, are created. For $30° < \theta < 80°$ with sufficiently large pressures, similar double layers are observed because the particle density can be high with the structure.

For $\theta \geq 90°$ or $\chi \geq 0.5$, as the double layers of the simple hexagonal lattice are not created, ϕ_6 is small irrespective of the pressure. In each layer, the mixture of a square lattice, which is the (100) face of the fcc lattice, and a triangular lattice, which is one of the bases of a simple hexagonal lattice, forms even in the high pressure region (Figures 13d and 14d). When the patch directions of all the particles are parallel to the *z*-axis for $\theta = 100°$ or $\chi = 5.9 \times 10^{-1}$, the number of connections per particle for the (100) face of the fcc lattice is fourteen: the particles connect with eight neighbors in the same layer and six neighbors in a different layer. On the other hand, the number of connections per particle for the simple hexagonal lattice is thirteen; particles connect six neighbors in the same layer and seven neighbors in a different layer. The number of connections per particle in the square lattice, which is the (100) face of the fcc structure, is larger than that in the triangular lattice, which is the basal plane of the simple hexagonal lattice. The internal energy per particle in the square lattice U_{fcc} is estimated as $U_{fcc} = -7\epsilon$, and that in the triangular lattice U_{hP} is estimated as $U_{hP} = -13\epsilon/2$. Thus, owing to the benefit of energy gain, the double layers of the square structure become dominant in high pressures.

CONCLUSIONS

In this paper, MC simulations were performed and the clusters and structures formed by one-patch particles in a thin system were studied. In the isothermal−isochoric simulations, the type of numerous clusters changed into dimers, tetrahedral tetramers, octahedral hexamers, and pentagonal dipyramidal heptamers with the increase of the patch area for a short interaction length. Taking into account the increase in the connections between particles, it is natural that the cluster size increased with increasing patch area. When the patch area was increased further, the string-like clusters which consist of the connections of the pentagonal dipyramidal heptamers formed. Finally, the double layers of island-like clusters, in which the direction of the patch area of almost all the particles is parallel to the *z*-axis, were created when $\theta = 100°$ or $\chi = 5.9 \times 10^{-1}$.

For the long interaction length, the cluster size also increased with increasing patch area, but different types of clusters were created: pentagonal bipyramidal heptamers did not form, but triangular prismatic hexamers formed. When $\Delta > \sqrt{3}\sigma$, the particles in the diagonal positions in a regular hexahedron with the lattice constant σ can attract each other. Thus, one can expect that the hexahedral octamers probably form to increase the energy gain.

The difference in the interaction length also affected the structures in the isothermal−isobaric systems. For the short interaction length, the double layers of a triangular lattice, which were the (111) face of the fcc lattice, formed when the pressure was high. When θ was around 70°, the double layers of triangular lattice were difficult to form, which was because the pentagonal dipyramidal heptamers observed in the isothermal isochoric simulations were stable. Probably, much higher pressure is needed to turn the system with pentagonal dipyramidal heptamers into a simple hexagonal structure. For the long interaction length, the double layers of the simple hexagonal lattice did not form when $\theta \geq 90°$. Instead of this structure, the double layers of a square lattice, which is the (100) face of the fcc lattice, were created to increase the energy gains. As the difference in the interaction energies per particles between the two structures was small, the mixture of the two structures was created in my simulations. However, only the double layers of the square lattice can be created if the pressure is higher. In these simulations, the interaction energy was set to $\epsilon/k_B T \leq 8.0$, which is not so large compared with that of the experiment,[12] but the system size was not large. Thus, one cannot completely wipe away the concern that the systems were trapped in quasistable states. To avoid the possibility that the systems did not reach the equilibrium states, it might be better to use other algorithms[14,19,21,61−64]

In these simulations, the width between the two walls l_z was set to 2.1σ. The restriction in the *z*-direction affected the orientation of clusters. For example, one of the triangular planes in octahedral hexamers and the pentagonal plane in the pentagonal dipyramidal heptamers which were observed for the short interaction length were almost parallel to the *xy*-plane. When l_z was thinner than that in the simulations, the orientation of other clusters can be probably controlled. The direction of the basal plane in the trigonal prismatic hexamer, which is observed in Figure 6a, may be restricted to the *xy*-plane. In Figure 6c, clusters such as C and D formed, but only clusters such as C are probably created in a thinner system.

Even for systems where the interaction between particles is simple and isotropic, structures created in thin systems constructed by two parallel walls are strongly affected by the width between the two walls.[54−59] Structures which are not expected from the free three-dimensional system are created in both experiments and simulations. When the attraction is anisotropic like patchy particles, more various unique structures may form when l_z is controlled. The author intended to study how the cluster shapes and structures formed by patchy particles depend on l_z.

COMPUTATIONAL METHODS

As shown in Figure 15, spherical patchy particles with one patch on their surface constructed in two parallel walls were considered. It is assumed that the interaction between the particles and the walls is hard-core repulsion. The interaction potential between particles is given by the KF potential; the interaction potential between the *i*th and *j*th particles, $U^{KF}(r_{ij})$, is expressed as[34]

$$U^{KF}(r_{ij}) = U_{rep}(r_{ij}) + U_{att}(r_{ij}) f(\hat{\boldsymbol{r}}_{ij}, \hat{\boldsymbol{n}}_i, \hat{\boldsymbol{n}}_j) \quad (2)$$

where $\boldsymbol{r}_i$ denotes the center of mass for the *i*th particle, $\boldsymbol{r}_{ij} = \boldsymbol{r}_j - \boldsymbol{r}_i$, $r_{ij} = |\boldsymbol{r}_{ij}|$, and $\hat{\boldsymbol{r}}_{ij} = \boldsymbol{r}_{ij}/r_{ij}$. The first term $U_{rep}(r_{ij})$ represents the hard-core repulsive potential given by

https://dx.doi.org/10.1021/acsomega.0c04159
ACS Omega XXXX, XXX, XXX−XXX

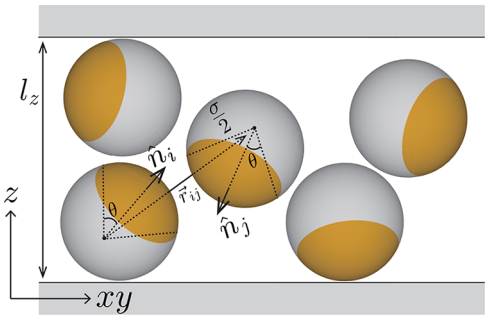

Figure 15. One-patch particles between two parallel walls. Orange area is the patch area which causes the attractive interaction between particles. The *xy*-plane is parallel to the walls and the *z*-axis is perpendicular to them.

$$U_{\mathrm{rep}}(r_{ij}) = \begin{cases} \infty & (r_{ij} \le \sigma) \\ 0 & (\sigma < r_{ij}) \end{cases} \tag{3}$$

where σ is the diameter of spherical patchy particles. The second term in eq 2 represents the attractive part in the KF potential. $U_{\mathrm{att}}(r_{ij})$ is the square-well potential given by

$$U_{\mathrm{att}}(r_{ij}) = \begin{cases} -\epsilon & (\sigma < r_{ij} \le \sigma + \Delta) \\ 0 & (\sigma + \Delta < r_{ij}) \end{cases} \tag{4}$$

where ϵ is the positive parameter representing the strength of attraction and Δ is the interaction length. The anisotropy of attraction caused by the patch area is given by $f(r_{ij},\hat{\boldsymbol{n}}_i,\hat{\boldsymbol{n}}_j)$, which is defined as

$$f(\hat{\boldsymbol{r}}_{ij}, \hat{\boldsymbol{n}}_i, \hat{\boldsymbol{n}}_j) = \begin{cases} 1 & (\hat{\boldsymbol{n}}_i \cdot \hat{\boldsymbol{r}}_{ij} > \cos\theta \text{ and } \hat{\boldsymbol{n}}_j \cdot \hat{\boldsymbol{r}}_{ji} > \cos\theta) \\ 0 & \text{otherwise} \end{cases} \tag{5}$$

When the diameter of patchy particles is σ, the patch area S is estimated as $S = \pi\sigma^2(1 - \cos\theta)/2$. The ratio of patch area on the whole surface χ is related to θ as $\chi = (1 - \cos\theta)/2$. χ changed from 3.0×10^{-1} to 5.9×10^{-2} as θ was changed from 20 and 100°.

AUTHOR INFORMATION

Corresponding Author

Masahide Sato − *Information Media Center, Kanazawa University, Kanazawa 920-1192, Japan;* orcid.org/0000-0001-8298-9016; Email: msato002@staff.kanazawa-u.ac.jp

Complete contact information is available at: https://pubs.acs.org/10.1021/acsomega.0c04159

Notes

The author declares no competing financial interest.

ACKNOWLEDGMENTS

This work was supported by JSPS KAKENHI Grant nos. JP20K03782, JP18K04960, and JP18H03839 and by the Grant for Joint Research Program of the Institute of Low Temperature Science, Hokkaido University, grant number 20G029.

REFERENCES

(1) Gong, Z.; Hueckel, T.; Yi, G.-R.; Sacanna, S. Patchy particles made by colloidal fusion. *Nature* **2017**, *550*, 234−238.

(2) Bianchi, E.; Largo, J.; Tartaglia, P.; Zaccarelli, E.; Sciortino, F. Phase Diagram of Patchy Colloids: Towards Empty Liquids. *Phys. Rev. Lett.* **2006**, *97*, 168301.

(3) Hong, L.; Cacciuto, A.; Luijten, E.; Granick, S. Clusters of Amphiphilic Colloidal Spheres. *Langmuir* **2008**, *24*, 621−625.

(4) Miller, W. L.; Cacciuto, A. Hierarchical self-assembly of asymmetric amphiphatic spherical colloidal particles. *Phys. Rev. E: Stat., Nonlinear, Soft Matter Phys.* **2009**, *80*, 021404.

(5) Sciortino, F.; Giacometti, A.; Pastore, G. Phase Diagram of Janus Particles. *Phys. Rev. Lett.* **2009**, *103*, 237801.

(6) Chen, Q.; Whitmer, J. K.; Jiang, S.; Bae, S. C.; Luijten, E.; Granick, S. Supracolloidal Reaction Kinetics of Janus Spheres. *Science* **2011**, *331*, 199−202.

(7) Chen, Q.; Bae, S. C.; Granick, S. Directed self-assembly of a colloidal kagome lattice. *Nature* **2011**, *469*, 381−384.

(8) Chen, Q.; Yan, J.; Zhang, J.; Bae, S. C.; Granick, S. Janus and Multiblock Colloidal Particles. *Langmuir* **2012**, *28*, 13555−13561.

(9) Romano, F.; Sanz, E.; Tartaglia, P.; Sciortino, F. Phase diagram of trivalent and pentavalent patchy particles. *J. Phys.: Condens. Matter* **2012**, *24*, 064113.

(10) Romano, F.; Sciortino, F. Patterning symmetry in the rational design of colloidal crystals. *Nat. Commun.* **2012**, *3*, 975.

(11) Wang, Y.; Wang, Y.; Breed, D. R.; Manoharan, V. N.; Feng, L.; Hollingsworth, A. D.; Weck, M.; Pine, D. J. Colloids with valence and specific directional bonding. *Nature* **2012**, *491*, 51−55.

(12) Iwashita, Y.; Kimura, Y. Stable cluster phase of Janus particles in two dimensions. *Soft Matter* **2013**, *9*, 10694−10968.

(13) Mao, X.; Chen, Q.; Granick, S. Entropy favours open colloidal lattices. *Nat. Mat.* **2013**, *12*, 217−222.

(14) Preisler, Z.; Vissers, T.; Smallenburg, F.; Munaò, G.; Sciortino, F. Phase Diagram of One-Patch Colloids Forming Tubes and Lamellae. *J. Phys. Chem. B* **2013**, *117*, 9540−9547.

(15) Vissers, T.; Preisler, Z.; Smallenburg, F.; Dijkstra, M.; Sciortino, F. Predicting crystals of Janus colloids. *J. Chem. Phys.* **2013**, *138*, 164505.

(16) Vissers, T.; Smallenburg, F.; Munaò, G.; Preisler, Z.; Sciortino, F. Cooperative polymerization of one-patch colloids. *J. Chem. Phys.* **2014**, *140*, 144902.

(17) Iwashita, Y.; Kimura, Y. Orientational order of one-patch colloidal particles in two dimensions. *Soft Matter* **2014**, *10*, 7170−7181.

(18) Shin, H.; Schweizer, K. S. Theory of two-dimensional self-assembly of Janus colloids: crystallization and orientational ordering. *Soft Matter* **2014**, *10*, 262−274.

(19) Preisler, Z.; Vissers, T.; Munaò, G.; Smallenburg, F.; Sciortino, F. Equilibrium phases of one-patch colloids with short-range attractions. *Soft Matter* **2014**, *10*, 5121−5128.

(20) Iwashita, Y.; Kimura, Y. Spatial confinement governs orientational order in patchy particles. *Sci. Rep.* **2016**, *6*, 27599.

(21) Preisler, Z.; Vissers, T.; Smallenburg, F.; Sciortino, F. Crystals of Janus colloids at various interaction ranges. *J. Chem. Phys.* **2016**, *145*, 064513.

(22) Reinhart, W. F.; Panagiotopoulos, A. Z. Equilibrium crystal phases of triblock Janus colloids. *J. Chem. Phys.* **2016**, *145*, 094505.

(23) Bianchi, E.; van Oostrum, P. D. J.; Likos, C. N.; Kahl, G. Inverse patchy colloids: Synthesis, modeling and self-organization. *Curr. Opin. Colloid Interface Sci.* **2017**, *30*, 8−15.

(24) Iwashita, Y.; Kimura, Y. Density dependence of orientational order in one-patch particles. *Soft Matter* **2017**, *13*, 4997−5007.

(25) Patra, N.; Tkachenko, A. V. Layer-by-layer assembly of patchy particles as a route to nontrivial structures. *Phys. Rev. E: Stat., Nonlinear, Soft Matter Phys.* **2017**, *96*, 022601.

(26) Ravaine, S.; Duguet, E. Synthesis and assembly of patchy particles: Recent progress and future prospects. *Curr. Opin. Colloid Interface Sci.* **2017**, *30*, 45−53.

(27) Reinhart, W. F.; Panagiotopoulos, A. Z. Directed assembly of photonic crystals through simple substrate patterning. *J. Chem. Phys.* **2019**, *150*, 014503.

https://dx.doi.org/10.1021/acsomega.0c04159
ACS Omega XXXX, XXX, XXX−XXX

(28) Cerbelaud, M.; Lebdioua, K.; Tran, C. T.; Crespin, B.; Aimable, A.; Videcoq, A. Brownian dynamics simulations of one-patch inverse patchy particles. *Phys. Chem. Chem. Phys.* **2019**, *21*, 23447−23458.
(29) Noguchi, T. G.; Iwashita, Y.; Kimura, Y. Controlled armoring of metal surfaces with metallodielectric patchy particles. *J. Chem. Phys.* **2019**, *150*, 174903.
(30) Oh, J. S.; Lee, S.; Glotzer, S. C.; Yi, G.-R.; Pine, D. J. Colloidal fibers and rings by cooperative assembly. *Nat. Commun.* **2019**, *10*, 3936.
(31) A, J. A. D.; Oh, J. S.; Yi, G.-R.; Pine, D. J. Photo-printing of faceted DNA patchy particles. *Proc. Natl. Acad. Sci. U.S.A.* **2020**, *117*, 10645−10653.
(32) Morphew, D.; Shaw, J.; Avins, C.; Chakrabarti, D. Programming Hierarchical Self-Assembly of Patchy Particles into Colloidal Crystals via Colloidal Molecules. *ACS Nano* **2018**, *12*, 2355−2364.
(33) Rao, A. B.; Shaw, J.; Neophytou, A.; Morphew, D.; Sciortino, F.; Johnston, R. L.; Chakrabarti, D. Leveraging Hierarchical Self-Assembly Pathways for Realizing Colloidal Photonic Crystals. *ACS Nano* **2020**, *14*, 5348−5359.
(34) Kern, N.; Frenkel, D. Fluid-fluid coexistence in colloidal systems with short-ranged strongly directional attraction. *J. Chem. Phys.* **2003**, *118*, 9882.
(35) Sato, M. Self-Assembly Formed by Spherical Patchy Particles with Long-Range Attraction. *J. Phys. Soc. Jpn.* **2019**, *88*, 104801.
(36) Mirkin, C. A.; Letsinger, R. L.; Mucic, R. C.; Storhoff, J. J. A DNA-based method for rationally assembling nanoparticles into macroscopic materials. *Nature* **1996**, *382*, 607−609.
(37) Nykypanchuk, D.; Maye, M. M.; van der Lelie, D.; Gang, O. DNA-guided crystallization of colloidal nanoparticles. *Nature* **2008**, *451*, 549−552.
(38) Park, S. Y.; Lytton-Jean, A. K. R.; Lee, B.; Weigand, S.; Schatz, G. C.; Mirkin, C. A. DNA-programmable nanoparticle crystallization. *Nature* **2008**, *451*, 553−556.
(39) Xiong, H.; Lelie, D. v. d.; Gang, O. Phase Behavior of Nanoparticles Assembled by DNA Linkers. *Phys. Rev. Lett.* **2009**, *102*, 015504.
(40) Macfarlane, R. J.; Lee, B.; Hill, H. D.; Senesi, A. J.; Seifert, S.; Mirkin, C. A. Assembly and organization processes in DNA-directed colloidal crystallization. *Proc. Natl. Acad. Sci. U.S.A.* **2009**, *106*, 10493−10498.
(41) Jones, M. R.; Macfarlane, R. J.; Lee, B.; Zhang, J.; Young, K. L.; Senesi, A. J.; Mirkin, C. A. DNA-nanoparticle superlattices formed from anisotropic building blocks. *Nat. Mater.* **2010**, *9*, 913−917.
(42) Cigler, P.; Lytton-Jean, A. K. R.; Anderson, D. G.; Finn, M. G.; Park, S. Y. DNA-controlled assembly of a NaTl lattice structure from gold nanoparticles and protein nanoparticles. *Nat. Mater.* **2010**, *9*, 918−922.
(43) Macfarlane, R. J.; Lee, B.; Jones, M. R.; Harris, N.; Schatz, G. C.; Mirkin, C. A. Nanoparticle Superlattice Engineering with DNA. *Science* **2011**, *334*, 204−208.
(44) Knorowski, C.; Burleigh, S.; Travesset, A. Dynamics and Statics of DNA-Programmable Nanoparticle Self-Assembly and Crystallization. *Phys. Rev. Lett.* **2011**, *106*, 215501.
(45) Rogers, W. B.; Crocker, J. C. Direct measurements of DNA-mediated colloidal interactions and their quantitative modeling. *Proc. Natl. Acad. Sci. U.S.A.* **2011**, *108*, 15687−15692.
(46) Zhang, C.; Macfarlane, R. J.; Young, K. L.; Choi, C. H. J.; Hao, L.; Auyeung, E.; Liu, G.; Zhou, X.; Mirkin, C. A. A general approach to DNA-programmable atom equivalents. *Nat. Mater.* **2013**, *12*, 741−746.
(47) Li, T. I. N. G.; Sknepnek, R.; Olvera de la Cruz, M. Thermally Active Hybridization Drives the Crystallization of DNA-Functionalized Nanoparticles. *J. Am. Chem. Soc.* **2013**, *135*, 8535−8541.
(48) Di Michele, L.; Varrato, F.; Kotar, J.; Nathan, S. H.; Foffi, G.; Eiser, E. Multistep kinetic self-assembly of DNA-coated colloids. *Nat. Commun.* **2013**, *4*, 2007.
(49) Srivastava, S.; Nykypanchuk, D.; Fukuto, M.; Halverson, J. D.; Tkachenko, A. V.; Yager, K. G.; Gang, O. Two-Dimensional DNA-Programmable Assembly of Nanoparticles at Liquid Interfaces. *J. Am. Chem. Soc.* **2014**, *136*, 8323−8332.
(50) Isogai, T.; Akada, E.; Nakada, S.; Yoshida, N.; Tero, R.; Harada, S.; Ujihara, T.; Tagawa, M. Effect of magnesium ion concentration on two-dimensional structure of DNA-functionalized nanoparticles on supported lipid bilayer. *Jpn. J. Appl. Phys.* **2016**, *55*, 03DF11.
(51) Katsuno, H.; Maegawa, Y.; Sato, M. Two-Dimensional Crystal Structure Formed by Two Components of DNA Nanoparticles on a Substrate. *J. Phys. Soc. Jpn.* **2016**, *85*, 074605.
(52) Pretti, E.; Zerze, H.; Song, M.; Ding, Y.; Mahynski, N. A.; Hatch, H. W.; Shen, V. K.; Mittal, J. Assembly of three-dimensional binary superlattices from multi-flavored particles. *Soft Matter* **2018**, *14*, 6303−6312.
(53) Wang, S.; Park, S. S.; Buru, C. T.; Lin, H.; Chen, P.-C.; Roth, E. W.; Farha, O. K.; Mirkin, C. A. Colloidal crystal engineering with metal-organic framework nanoparticles and DNA. *Nat. Commun.* **2020**, *11*, 2495.
(54) Schmidt, M.; Löwen, H. Phase diagram of hard spheres confined between two parallel plates. *Phys. Rev. E: Stat., Nonlinear, Soft Matter Phys.* **1997**, *55*, 7228−7241.
(55) Ramiro-Manzano, R.; Bonet, E.; Rodriguez, I.; Meseguer, F. Layering transitions in confined colloidal crystals: The hcp-like phase. *Phys. Rev. E: Stat., Nonlinear, Soft Matter Phys.* **2007**, *76*, 050401.
(56) Fontecha, A. B.; Palberg, T.; Schöpe, H. J. Construction and stability of a close-packed structure observed in thin colloidal crystals. *Phys. Rev. E: Stat., Nonlinear, Soft Matter Phys.* **2007**, *76*, 050402.
(57) Curk, T.; de Hoogh, A.; Martinez-Veracoechea, F. J.; Eiser, E.; Frenkel, D.; Dobnikar, J.; Leunissen, M. E. Layering, freezing, and re-entrant melting of hard spheres in soft confinement. *Phys. Rev. E: Stat., Nonlinear, Soft Matter Phys.* **2012**, *85*, 021502.
(58) Oğuz, E. C.; Reinmüller, A.; Schöpe, H. J.; Palberg, T.; Messina, R.; Löwen, H. Crystalline multilayers of charged colloids in soft confinement: experiment versus theory. *J. Phys. Condens. Matter* **2012**, *24*, 464123.
(59) Harth, K.; Mauney, A.; Stannarius, R. Frustrated packing of spheres in a flat container under symmetry-breaking bias. *Phys. Rev. E: Stat., Nonlinear, Soft Matter Phys.* **2015**, *91*, 030201.
(60) Avvisati, G.; Vissers, T.; Dijkstra, M. Self-assembly of patchy colloidal dumbbells. *J. Chem. Phys.* **2015**, *142*, 084905.
(61) Chen, B.; Siepmann, J. I. Novel Monte Carlo Algorithm for Simulating Strongly Associating Fluids: Applications to Water, Hydrogen Fluoride, and Acetic Acid. *J. Phys. Chem. B* **2000**, *104*, 8725−8734.
(62) Filion, L.; Marechal, M.; van Oorschot, B.; Pelt, D.; Smallenburg, F.; Dijkstra, M. Efficient Method for Predicting Crystal Structures at Finite Temperature: Variable Box Shape Simulations. *Phys. Rev. Lett.* **2009**, *103*, 188302.
(63) de Graaf, J.; van Roij, R.; Dijkstra, M. Dense Regular Packings of Irregular Nonconvex Particles. *Phys. Rev. Lett.* **2011**, *107*, 155501.
(64) de Graaf, J.; Filion, L.; Marechal, M.; van Roij, R.; Dijkstra, M. Crystal-structure prediction via the Floppy-Box Monte Carlo algorithm: Method and application to hard (non)convex particles. *J. Chem. Phys.* **2012**, *137*, 214101.

https://dx.doi.org/10.1021/acsomega.0c04159
ACS Omega XXXX, XXX, XXX−XXX